

# Antiskid decay prediction of asphalt mixtures based on aggregate mechanical properties and gradation fractals

Kong Lingyun<sup>1,2</sup> Zeng Qilan<sup>1,2</sup> Zhang Zhengqi<sup>1,2</sup> Peng Yi<sup>3</sup>  
Wang Dawei<sup>4</sup> Yu Miao<sup>1,2</sup> Zhan You<sup>5</sup>

(<sup>1</sup>National and Local Joint Laboratory of Traffic Civil Engineering Materials, Chongqing Jiaotong University, Chongqing 400074, China)

(<sup>2</sup>School of Civil Engineering, Chongqing Jiaotong University, Chongqing 400074, China)

(<sup>3</sup>College of Traffic and Transportation, Chongqing Jiaotong University, Chongqing 400074, China)

(<sup>4</sup>School of Transportation Science and Engineering, Harbin Institute of Technology, Harbin 150090, China)

(<sup>5</sup>School of Civil Engineering, Southwest Jiaotong University, Chengdu 610031, China)

**Abstract:** Through comprehensive data collection, along with the coarse aggregate mechanical index, fractal dimension, and British pendulum number (BPN), a pavement friction prediction model was proposed on the basis of backpropagation neural networks (BPNNs) and support vector machine (SVM). An accelerated attenuation test was conducted to examine the antiskid performance of the asphalt mixture and aggregates at different wearing cycles. Subsequently, BPN was fitted using an exponential model. Gray relational and correlation analyses were performed to evaluate the factors influencing pavement skid resistance. According to the principal component analysis results, six schemes were prepared for the training, validation, and testing of BPNN and SVM algorithms. Test results indicate that different aggregates exhibit different antiskid properties. Quartz sandstone is the most suitable, followed by basalt and limestone. The polished stone value has the highest correlation with the attenuation model of asphalt antiskid performance. BPNN is more stable, with an  $R^2$  value of approximately 0.8.

**Key words:** accelerated loading; antiskid performance; exponential model; backpropagation neural networks (BPNN); support vector machine (SVM)

**DOI:** 10.3969/j.issn.1003-7985.2024.01.007

Skid resistance evaluation in pavement surfaces is a critical indicator of road safety<sup>[1-2]</sup>. A reduction in skid resistance below a certain threshold can significantly increase the risk of traffic accidents<sup>[3-4]</sup>. Low skid resistance may lead to an elevated risk of collisions, such as

sliding or rear-end crashes<sup>[5]</sup>. In addition, the selection of appropriate evaluation criteria to accurately assess and predict the antiskid performance of pavement is of utmost importance<sup>[6]</sup>.

Numerous factors affect the friction between a tire and pavement<sup>[7-8]</sup>. The micro- and macro-texture of the pavement are key components for its interaction with the tire<sup>[9]</sup>. Microtexture refers to irregularities in pavement surface dimensions, ranging from 0.001 to 0.5 mm vertically and less than 0.5 mm horizontally<sup>[10-11]</sup>. This texture is mainly associated with the roughness of aggregate surfaces<sup>[12-13]</sup>. Fractal geometry has gained popularity in image analysis and texture recognition for several decades because of its exceptional performance and versatility, particularly in analyzing the roughness of aggregate surfaces<sup>[14-15]</sup>. Its numerous applications make it a valuable tool in this field. The self-similarity in pavement microtopography allows the description of pavement texture using fractal theory, rendering it a viable approach<sup>[16-17]</sup>. Consequently, scholars have employed fractal interpolation to examine the connection between the fractal dimension and skid resistance<sup>[18-19]</sup>.

The repeated polishing of the surface texture by traffic results in a gradual decrease in skid resistance toward a long-term pavement in-service performance decay<sup>[20-22]</sup>. The long-term skid resistance of pavement surfaces relies on the capacity of aggregates to maintain their microtexture with polishing action<sup>[23]</sup>. Moreover, the mechanical properties of the aggregates can be used to assess their microtexture-retaining ability<sup>[24]</sup>. Yu et al.<sup>[25]</sup> analyzed the correlation between the mechanical properties of five types of aggregates and their skid resistance deterioration performance using gray relational analysis (GRA); results showed that the influence of aggregate properties on the final value of British pendulum number (BPN) was the chronological values of polished stone, hardness, crushed stone, impact, and abrasion. However, only a few studies have quantitatively evaluated the combined effects of the mechanical properties and gradation fractals of graded aggregates on pavement skid resistance.

**Received** 2023-07-21, **Revised** 2023-11-10.

**Biographies:** Kong Lingyun (1976—), female, doctor, professor; Peng Yi (corresponding author), male, doctor, dawsonyp@cqjtu.edu.cn.

**Foundation items:** National Natural Science Foundation of China (No. 52208425), Chongqing Postdoctoral Science Foundation (No. cstc2019jcyj-msxmX0744), China Postdoctoral Science Foundation (No. 2021M693918).

**Citation:** Kong Lingyun, Zeng Qilan, Zhang Zhengqi, et al. Antiskid decay prediction of asphalt mixtures based on aggregate mechanical properties and gradation fractals [J]. Journal of Southeast University (English Edition), 2024, 40(1): 58 – 67. DOI: 10.3969/j.issn.1003-7985.2024.01.007.

predict the impact of aggregate mechanical properties and gradation fractals on the skid resistance of asphalt pavement.

The influence of the mechanical characteristics of the aggregates on the anti-sliding performance was reasonably evaluated by selecting four aggregates with different lithologies, including limestone, basalt, granite, and quartz sandstone, for the test. As shown in Fig. 1, there are three types of limestone and two types of basalt according to the classification of material sources. Because the source of limestone was insufficient, limestone I was selected as the fine aggregate. Limestone powder was used as the filler.

[illegible]

1.4 Calculation of aggregate morphology features

The fractal dimension is the main index used to measure the complexity and irregularity of an object or fractal body. The fractal dimension of the grading curve was calculated using the Tyler’s three-dimensional (3D) fractal characteristic model of particle size<sup>[32]</sup>. The fractal relationship between particle mass and size is given as follows<sup>[33]</sup>:

lgm\_{r>d\_i} = (3 - D)(lgd\_i - lgd\_{max}) + lgm\_T \tag{1}

D = 3 - \frac{lgm\_{r>d\_i} - lgm\_T}{lgd\_i - lgd\_{max}} \tag{2}

where  $r$  and  $D$  denote the specified particle size and fractal dimension;  $d_i$  denotes the diameter of the  $i$ -th ( $i = 1, 2, 3$ ) particle obtained from the grading curve;  $m_{r>d_i}$  denotes the mass of the aggregate particle that did not pass through the sieve of  $d_i$  size;  $m_T$  denotes the sum of the

mass for all aggregates;  $d_{max}$  denotes the maximum of  $d_i$ .

1.5 Aggregate index

The crushing value data of the aggregates were obtained using a stone crushing value tester according to the T0316—2005 test method of *Highway Engineering Aggregate Test Regulations*. The abrasion value data of the aggregates were obtained using the Los Angeles Abrasion test method. Each aggregate was subjected to an abrasion test according to the T0317—2005 test method of *Highway Engineering Aggregate Test Regulations* by selecting the B-class particle size category. The polishing test was conducted according to the T0321—2005 test method of *Highway Engineering Aggregate Test Regulations*. An accelerated polishing test machine was used to process the aggregate, and the polishing value was measured using a pendulum instrument. The aggregate indices measured through experiments are listed in Table 3.

Table 3 Indexes of aggregates

Index	Limestone I	Limestone II	Limestone III	Basalt I	Basalt II	Granite	Quartz sandstone
Crushed stone value	24.3	25.2	20.6	11.1	13	14.5	15
Abrasion value	21.8	20.2	20.69	7.9	9.8	10.1	13.17
Polished stone value	43.4	44.3	49.3	54.1	56.6	49.6	61.4
Fractal dimension	2.45-2.52	2.45-2.52	2.46-2.62	2.46-2.62	2.45-2.52	2.45-2.52	2.46-2.62
P <sub>1</sub>	30-37	30-37	27-47	27-47	30-37	27-47	27-47
P <sub>2</sub>	47-53	47-53	45-63	45-63	47-53	45-63	45-63
P <sub>3</sub>	74-82	74-82	75-84	75-84	74-82	75-84	75-84
P <sub>4</sub>	95-97	95-97	91-97	91-97	95-97	91-97	91-97

Note: P<sub>1</sub>, P<sub>2</sub>, P<sub>3</sub>, and P<sub>4</sub> represent percentage passing of 2.36, 4.75, 9.50, and 13.20 mm, respectively.

2 Accelerated Attenuation Test for Skid Resistance

The small-scale accelerated wear test equipment developed by the laboratory was used to simulate the traffic load cycle effect of the vehicle on the asphalt pavement to simulate the attenuation process of the antiskid performance of the asphalt pavement in less time.

The equipment parameters were a tire with a 100 mm width, 200 mm diameter, 25 mm thick tread rubber, 0.8

KN tire load, and 0.2 MPa contact stress between the tire and the ground. The four tires of the equipment rotated around the central axis at 60 r/min. The temperature of the test environment was 25 °C. The test flow chart is shown in Fig. 2. The number of accelerated wears was set to 0, 1.2 × 10<sup>4</sup>, 2.7 × 10<sup>4</sup>, 3.9 × 10<sup>4</sup>, 5.1 × 10<sup>4</sup>, 6.3 × 10<sup>4</sup>, 7.5 × 10<sup>4</sup>, 8.7 × 10<sup>4</sup>, 9.9 × 10<sup>4</sup>, and 1.1 × 10<sup>5</sup> times (10 levels). BPN values were collected using a pendulum tribometer after loading each level. The BPN test followed the China field test method T0964—2008.

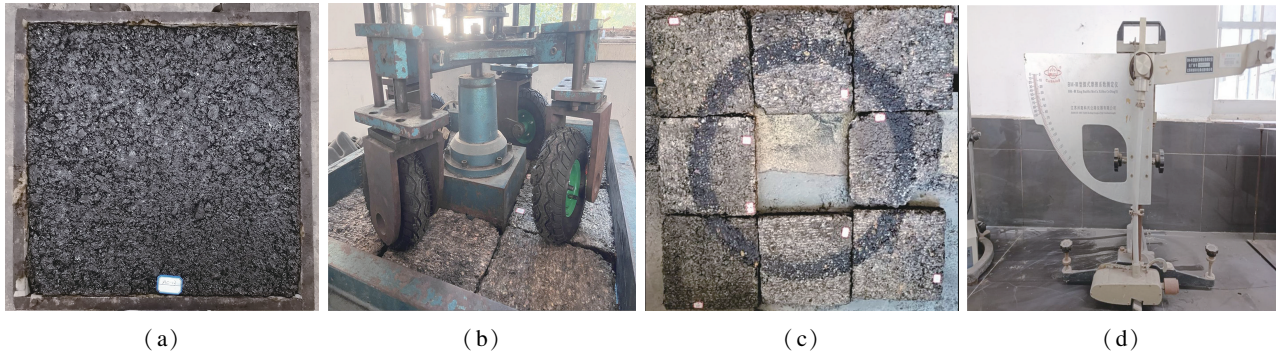


Fig. 2 Test flow chart. (a) Specimens; (b) Accelerated wear equipment; (c) Surface of specimens after loading; (d) BPN test

Studies have shown that the antiskid performance of asphalt pavement has an exponential attenuation process. Therefore, we used an exponential model to fit the asphalt mixture BPN data in different accelerated wear stages<sup>[8]</sup>,

$$\text{BPN} = ae^{-bx} + c \quad (3)$$

where  $a$ ,  $b$ , and  $c$  denote the loss value, loss rate, and terminal value of the BPN, respectively;  $x$  represents the number of wearing times.

### 3 BPNN and SVM

#### 3.1 BPNN algorithm

This study used the mechanical characteristics of the coarse aggregate, the fractal dimension of the gradation, and the passing rate of some apertures as pavement characteristics. In addition, the relationship between pavement characteristics and antiskid performance was established using the BPNN algorithm. BPNN comprises input, hidden, and output layers, which are connected by the connection weight  $W_k$ <sup>[34]</sup> (see Fig. 3). This study chose the bipolar S-type function as the activation function of the neurons in the hidden layer based on the non-linear relationship between the input and output layers.

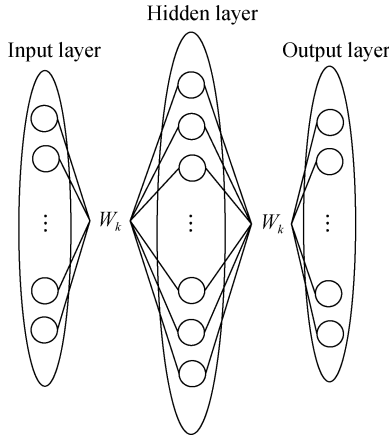


Fig. 3 Schematic of the BPNN model

#### 3.2 SVM algorithm

This study established the relationship between pavement characteristics and antiskid performance based on SVM, a binary classification model. The kernel function was used to map the inseparable low-dimensional space to a separable high-dimensional space. The dual variable was realized by introducing an insensitive function, sparsity, to establish an SVM regression model<sup>[35]</sup>.

#### 3.3 Evaluation index

We used the root mean square error (RMSE), mean absolute error (MAE), and coefficient of determination ( $R^2$ ) as evaluation indicators.

In addition to the conventional evaluation indicators, this study introduced the objective function (OBJ) as an evaluation indicator<sup>[36]</sup>:

$$O = \frac{n_t}{n_a} \frac{E_t + M_t}{R_t^2 + 1} + \frac{n_e}{n_a} \frac{E_e + M_e}{R_e^2 + 1} \quad (4)$$

where  $n_a$  denotes the number of data points in the training and test datasets;  $E_t$ ,  $M_t$ ,  $R_t^2$ , and  $n_t$  represent RMSE, MAE, coefficient of determination, and the number of data points in the training dataset;  $E_e$ ,  $M_e$ ,  $R_e^2$ , and  $n_e$  represent the RMSE, MAE, coefficient of determination, and the number of data points in the test dataset, respectively.

#### 3.4 Model construction

The antiskid performance of the pavement was predicted on the basis of the mechanical and morphological characteristics of the aggregates. The exponential model obtained by fitting the BPN data of the asphalt mixture represents the pavement skid resistance under load. The polishing value, crushing value, fractal dimension, and percentage passing were used as input variables. Furthermore, relevant parameters of the exponential model were taken as the response variables, 15 sample data points were selected as the training set, and the remaining 12 sample data points were selected as the test set to verify the model and establish the BPNN and SVM regression models.

Considering some features have similar effects on the antiskid performance of pavement<sup>[22]</sup>, principal component analysis (PCA) was used to extract components that independently characterize the pavement and take them as a class of input variables. Consequently, a better class of input variables was selected by comparing the model evaluation indicators using the original features and those obtained by PCA.

Furthermore, neurons in the output and hidden layers were set to one each for the BPNN algorithm. It was found through the loop verification method that 12 neurons could obtain better results. The initial weight and threshold range were  $(-1, 1)$ . The momentum factor and learning rate were set to 0.95 and 0.05, respectively, according to experience. The output layer used a purelin (linear) activation function with 1 slope and 0 intercept.

Furthermore, the SVM regression model was built on the Matlab<sup>®</sup> software platform. The fitsvm function was used to complete the least square optimization solution of the dual function, and cross-validation was used to verify the reliability of the model. The grid search algorithm was used to determine the optimal penalty factor and the parameter of the radial basis kernel function. The calculation met the requirements when the RMSE of the result did not exceed 0.001.



## 4 Results and Analysis

### 4.1 Accelerated attenuation test results for skid resistance

Fig. 4 shows the BPN attenuation curve at the asphalt mixture contact surface after the load was applied. The initial BPN values of the different aggregates differed. The initial BPN values of basalt I , basalt II , limestone I , limestone II , granite, and quartz sandstone were approximately 70, whereas the value was less than 60 for limestone III .

As the loading times increased, the asphalt mixture surface became gradually smoother, the antiskid performance gradually decreased, and the attenuation rate of different aggregates differed. Parameter  $b$  in Table 4 reflects the specific attenuation rate. The attenuation rates of the three limestone types were high under different gradations. The attenuation rates of limestones I and II were concentrat-

ed at 0.77 to 0.72 , which is greater than the decay rate of limestone III ( between 0.64 and 0.43 ) . The attenuation rates of the other aggregates were lower than those of limestone. Quartz sandstone, the most prominent aggregate, had an attenuation rate concentrated between 0.17 and 0.13.

Moreover, the attenuation of the BPN value was stable when the loading times exceeded 60 000. For BPN = 50 as the dividing line, the final BPN values of the quartz sandstone aggregates were above it. However, the final BPN values of the basalt and granite aggregates were approximately 50 and less than 50 for the limestone aggregates.

Thus, quartz sandstone exhibited the best antiskid performance, granite and basalt exhibited similar performance, and limestone exhibited the worst performance. Moreover, the antiskid performance of the different limestone types differed.

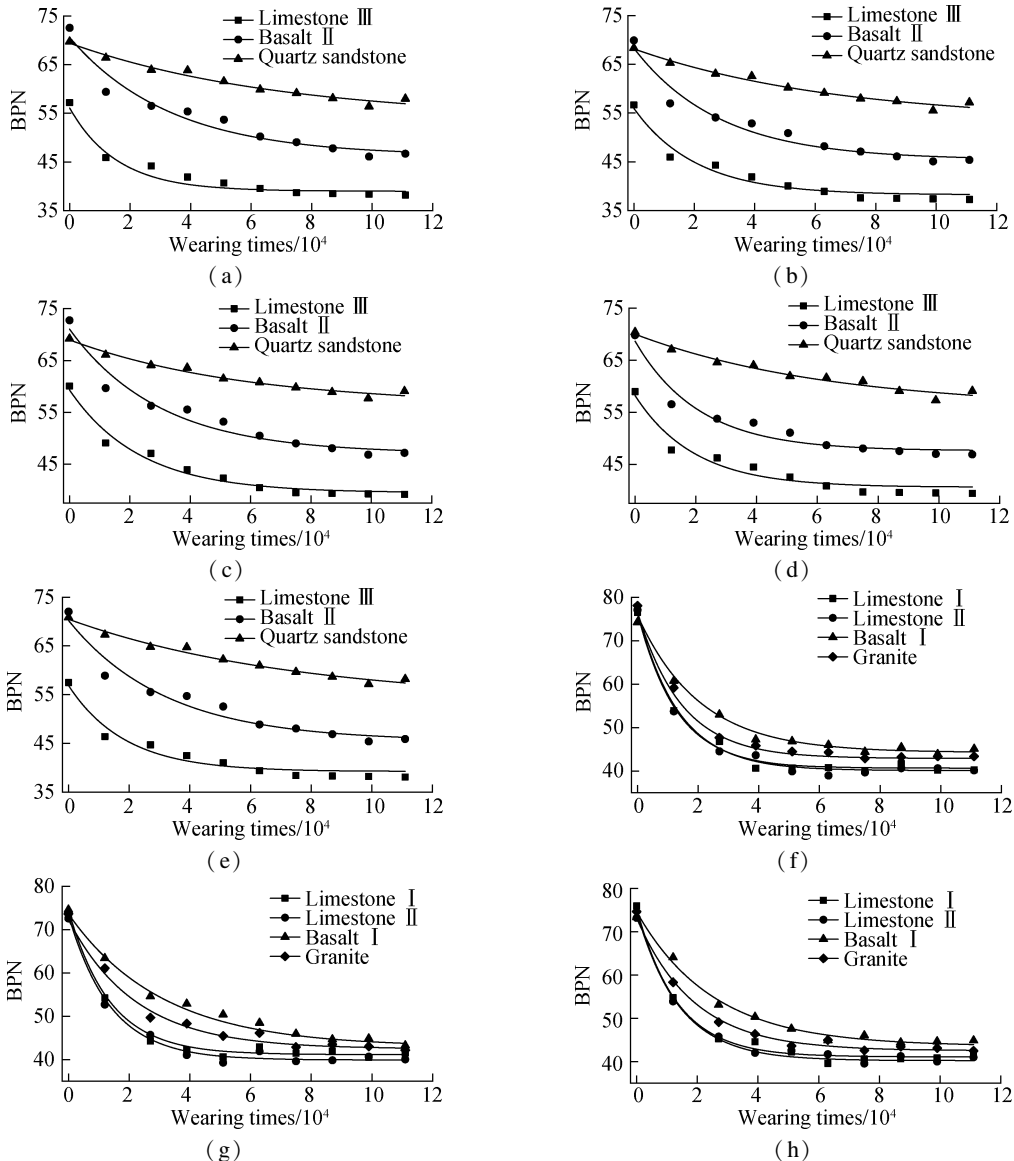


**Fig. 4** Exponential model and data of the accelerated attenuation tests. (a) Gradation 1; (b) Gradation 2; (c) Gradation 3; (d) Gradation 4; (e) Gradation 5; (f) Gradation 6; (g) Gradation 7; (h) Gradation 8

Table 4 Exponential model parameters

Gradation	Type of aggregate	Parameter		
		<i>a</i>	<i>b</i>	<i>c</i>
1	Limestone III	17.09	0.64	39.65
	Basalt II	24.39	0.30	46.20
	Quartz sandstone	15.65	0.14	53.79
2	Limestone III	17.73	0.49	38.23
	Basalt II	22.90	0.35	45.41
	Quartz sandstone	14.88	0.15	53.28
3	Limestone III	19.79	0.43	39.51
	Basalt II	23.98	0.33	47.06
	Quartz sandstone	12.64	0.17	56.32
4	Limestone III	17.59	0.51	40.61
	Basalt II	21.04	0.47	47.61
	Quartz sandstone	14.27	0.16	55.71
5	Limestone III	17.62	0.54	39.23
	Basalt II	24.76	0.31	45.45
	Quartz sandstone	16.92	0.13	53.55
6	Limestone I	35.70	0.77	40.65
	Limestone II	36.34	0.73	40.09
	Basalt I	31.59	0.49	44.25
	Granite	33.66	0.69	42.89
7	Limestone I	33.35	0.73	41.15
	Limestone II	33.47	0.72	39.90
	Basalt I	30.73	0.33	42.91
	Granite	29.86	0.45	42.46
8	Limestone I	34.17	0.75	41.09
	Limestone II	34.31	0.72	40.21
	Basalt I	30.99	0.40	43.56
	Granite	30.62	0.53	42.51

4.2 GRA results

GRA is a multifactor statistical analysis method used to analyze the correlation between multiple independent and dependent variables<sup>[21]</sup>. As shown in Fig. 5, the correlation degree was calculated by considering parameters *a*,

*b*, and *c* as the reference sequence and comparing them with the indicators listed in Table 3 and the partial percent passing of each gradation. The correlation between the polishing value and the three parameters was the strongest. The correlation degrees of the four features related to gradation were similar and above 0.6. The abrasion values were weakly correlated with the crushing values.

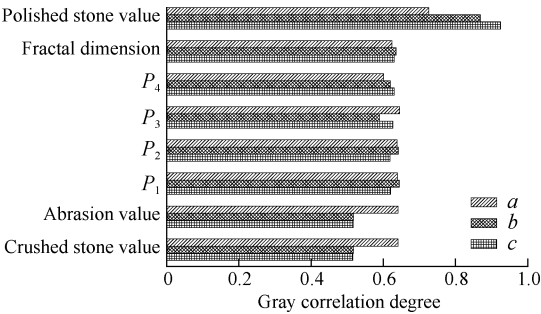


Fig. 5 GRA results

4.3 Correlation analysis results

The gray correlation analysis showed that the correlation coefficient of each factor exceeded 0.5. Therefore, each factor can affect the skid resistance of long-term service asphalt pavement to a certain extent, implying a high correlation between various factors<sup>[37]</sup>. Correlation analysis between various factors was performed. The results are shown in Table 5.

Table 5 shows that the correlation between the indicators representing the mechanical characteristics of aggregates, the fractal dimension representing the characteristics of the grading curve, and the pore diameter passing rate are more than 0.8, agreeing with the actual situation and indicating that the correlation analysis results can be improved.

Table 5 Correlation analysis results

Index	Crushed stone value	Abrasion value	Polished stone value	Fractal dimension	<i>P</i> <sub>1</sub>	<i>P</i> <sub>2</sub>	<i>P</i> <sub>3</sub>	<i>P</i> <sub>4</sub>
Crushed stone value	1.00	0.96	−0.76	−0.14	−0.11	−0.12	−0.17	0.17
Abrasion value	0.96	1.00	−0.64	−0.05	−0.04	−0.05	−0.07	0.07
Polished stone value	−0.76	−0.64	1.00	0.20	0.16	0.17	0.25	−0.25
Fractal dimension	−0.14	−0.05	0.20	1.00	0.95	0.97	0.41	−0.11
<i>P</i> <sub>1</sub>	−0.11	−0.04	0.16	0.95	1.00	0.99	0.12	−0.26
<i>P</i> <sub>2</sub>	−0.12	−0.05	0.17	0.97	0.99	1.00	0.21	−0.23
<i>P</i> <sub>3</sub>	−0.17	−0.07	0.25	0.41	0.12	0.21	1.00	0.27
<i>P</i> <sub>4</sub>	0.17	0.07	−0.25	−0.11	−0.26	−0.23	0.27	1.00

4.4 Principal component analysis results

The correlation analysis results showed a high degree of correlation between the input layer parts. Considering the practical significance of variables such as fractal dimension, percent passing, crushing value, and wear value, we performed PCA to obtain variables that can independently characterize the antiskid performance of pavement<sup>[38]</sup>; the PCA results are presented in Table 6.

Using components 1, 2, and 3 as comprehensive variables to represent all original variables, we can explain 89.5% variance. According to the composition matrix, the crushing, abrasion, and polishing values mainly constitute component 2. The fractal dimension and percent passing of 2.36 and 4.75 mm mainly constitute component 1; the percent passing of 9.50 and 13.20 mm mainly constitute component 3. Furthermore, this result is roughly the same as the correlation between the variables

Table 6 Component matrix

Index	1	2	3	4	5	6
Crushed stone value	0	0.966	0	0.258	0	0
Abrasion value	0	0.966	0	0.259	0	0
Polished stone value	0	-0.695	0	0.719	0	0
Fractal dimension	0.999	0	-0.009	0	-0.012	-0.036
$P_1$	0.956	0	-0.292	0	-0.015	0.034
$P_2$	0.961	0	-0.272	0	0.040	0.001
$P_3$	0.325	0	0.895	0	-0.305	0.005
$P_4$	0.285	0	0.908	0	0.308	0.005

presented by the correlation analysis, making it credible.

Finally, the three combinations of input features selected using the analysis of all characteristic variables are as follows:

- 1) All features were used as the input layer.
- 2) Polishing value, fractal dimension, 9.50 mm aperture pass rate, and 13.20 mm aperture pass rate, which are features highly related to antiskid performance, were used as the input layer.
- 3) Components 1, 2, and 3 obtained from PCA were used as the input layer.

4.5 Model selection and performance

In Table 7, we paired BPNN and SVM algorithms and the combination of the three input layers to construct a prediction model for parameters  $a$ ,  $b$ , and  $c$  in the attenuation model.

Table 7 Model building schemes

Input layer combination	$a$		$b$		$c$	
	BPNN	SVM	BPNN	SVM	BPNN	SVM
1	a-B-1	a-S-1	b-B-1	b-S-1	c-B-1	c-S-1
2	a-B-2	a-S-2	b-B-2	b-S-2	c-B-2	c-S-2
3	a-B-3	a-S-3	b-B-3	b-S-3	c-B-3	c-S-3

The performance of the different schemes for predicting the three parameters is shown in Table 8.

Table 8 Performance of different schemes

Scheme	$R^2$		OBJ
	Train database	Test database	
a-B-1	0.606	0.854	8.077
a-B-2	0.813	0.743	8.384
a-B-3	0.278	0.820	11.678
a-S-1	0.909	0.228	12.490
a-S-2	0.198	0.756	33.729
a-S-3	0.101	0.581	12.769
b-B-1	0.983	0.826	0.064
b-B-2	0.822	0.903	0.071
b-B-3	0.489	0.817	0.185
b-S-1	0.899	0.844	40.150
b-S-2	0.898	0.806	40.429
b-S-3	0.477	0.830	48.153
c-B-1	0.974	0.809	1.973
c-B-2	0.965	0.817	2.462
c-B-3	0.469	0.772	7.191
c-S-1	0.990	0.830	5.431
c-S-2	0.989	0.811	5.384
c-S-3	0.555	0.808	5.084

The BPNN algorithm and combination 1 had the best prediction effect on the three parameters. It had a higher  $R^2$  value, and its OBJ values of 8.08, 0.06, and 1.97 were the lowest for different models compared with the same parameter. The model with combination 3 as the input layer had a significantly larger OBJ value than that with combinations 1 and 2, and its  $R^2$  was less than 0.5. When these characteristics were summarized by PCA, the influence of some features on the three parameters was lost, resulting in poor prediction results. The differences in  $R^2$  and OBJ for combinations 1 and 2 as the input layer were small. Moreover, some low correlations were excluded when analyzing the correlation between different features and the output layer. These features had little effect on the prediction performance of the model.  $R^2$  was similar for combinations using SVM and BPNN. However, combinations using SVM had larger OBJ than those using BPNN. Therefore, we selected three combinations of a-B-1, b-B-1, and c-B-1 as the prediction models for parameters  $a$ ,  $b$ , and  $c$ , respectively (see Fig. 6).

5 Conclusions

1) The different aggregates exhibited different antiskid properties as the number of loadings increased. The attenuation rate of quartz sandstone, which exhibited the best antiskid performance, was concentrated between 0.17 and 0.13, and its BPN value was stable above 50. The attenuation rates of the two types of basalt and granite were between 0.53 and 0.30, and their BPN values were stable at 50, indicating similar antiskid properties. However, the attenuation rates of the three types of limestone were high, and their BPN values were less than 50 after stabilization, indicating that the antiskid properties were not good.

2) The gray correlation between the grinding value of the mechanical and morphological characteristics of the aggregate and the attenuation model of asphalt antiskid performance was the highest. Moreover, the correlation coefficients with the three parameters exceeded 0.85, indicating a high correlation. After summarizing all characteristics into three main components, component 2 comprised polishing, abrasion, and crushing values, reflecting the mechanical characteristics of the aggregate. The remaining two main components were the fractal dimension and pore passing rate, reflecting the aggregate morphology.

3) The model was constructed with three input layer combinations using BPNN and SVM algorithms. After comparing the evaluation indicators of different models, the prediction effect of different input layer combinations according to the BPNN model was more stable, with an  $R^2$  value of approximately 0.8. The combinations of a-B-1, b-B-1, and c-B-1 were selected and used as prediction models for parameters  $a$ ,  $b$ , and  $c$ . This selection result

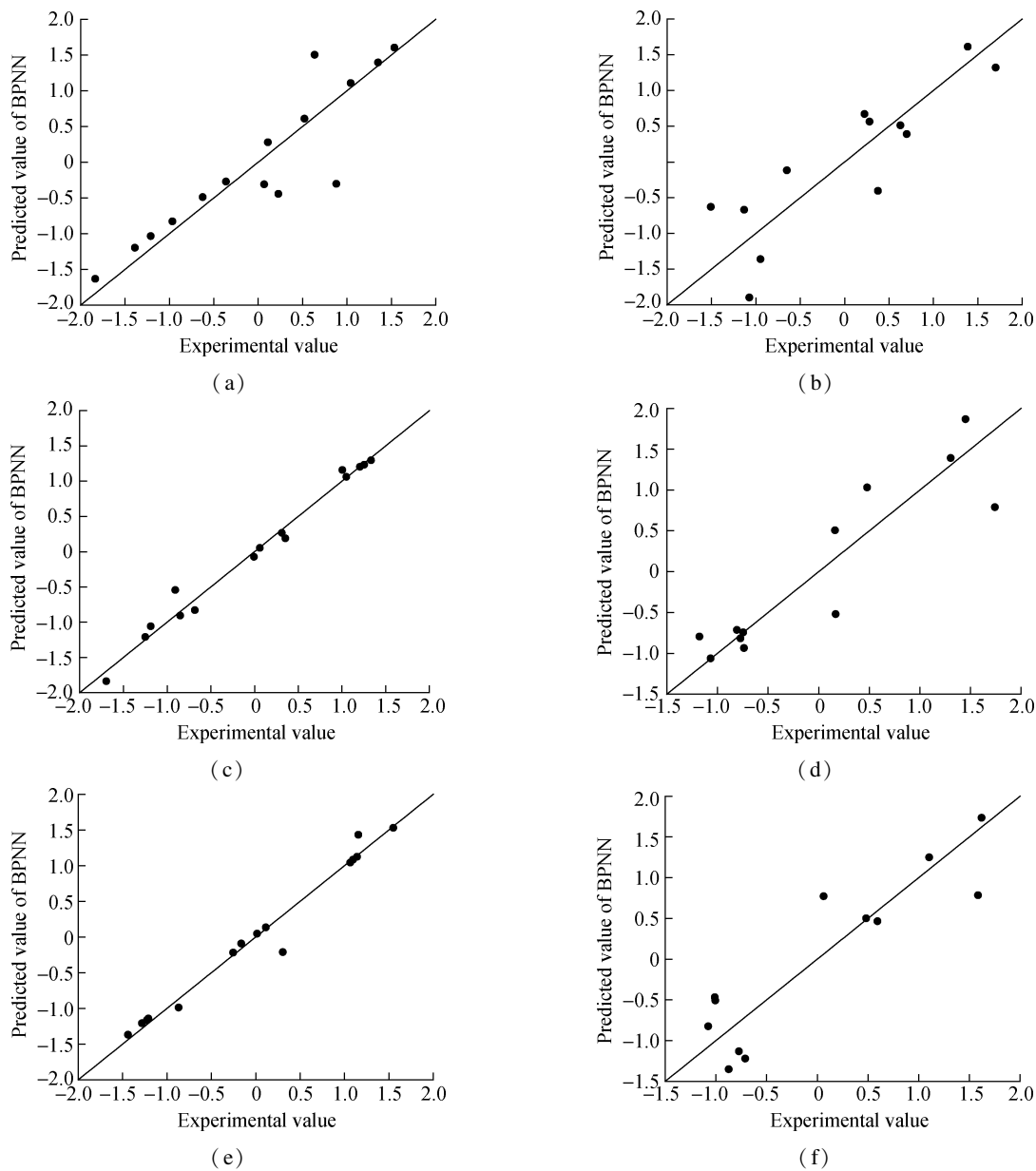


**Fig. 6** Evaluation of the results for three combinations. (a) Training dataset for a-B-1; (b) Test dataset for a-B-1; (c) Training dataset for b-B-1; (d) Test dataset for a-B-1; (e) Training dataset for c-B-1; (f) Test dataset for a-B-1

showed that features, excluding those with a low correlation, significantly affected the prediction effect of the model.

References

[1] Kane M, Lim M, Do T M, et al. A new predictive skid resistance model (PSRM) for pavement evolution due to texture polishing by traffic [J]. *Construction and Building Materials*, 2022, **342**: 128052. DOI: 10.1016/j.conbuildmat.2022.128052.

[2] Ueckermann A, Wang D, Oeser M, et al. Calculation of skid resistance from texture measurements [J]. *Journal of Traffic and Transportation Engineering (English Edition)*, 2015, **2**(1): 3 – 16. DOI: 10.1016/j.jtte.2015.01.001.

[3] Fwa T F. Skid resistance determination for pavement

management and wet-weather road safety [J]. *International Journal of Transportation Science and Technology*, 2017, **6**(3): 217 – 227. DOI: 10.1016/j.ijtst.2017.08.001.

[4] Zheng B, Zhu S, Cheng Y, et al. Analysis on influence factors of adhesion characteristic of tire-asphalt pavement based on tire hydroplaning model[J]. *Journal of South-east University (Natural Science Edition)*, 2018, **48**(4): 719 – 725. DOI: 10.3969/j.issn.1001-0505.2018.04.019. (in Chinese)

[5] Grande Z, Castillo E, Mora E, et al. Highway and road probabilistic safety assessment based on Bayesian network models [J]. *Computer-Aided Civil and Infrastructure Engineering*, 2017, **32**(5): 379 – 396. DOI: 10.1111/mice.12248.

[6] Liu C, Du Y, Wong S, et al. Eco-based pavement life-cycle maintenance scheduling optimization for equilibrated



- networks [J]. *Transportation Research Part D: Transport and Environment*, 2020, **86**: 102471. DOI: 10.1016/j.trd.2020.102471.
- [7] Lei J a, Zheng N, Chen X, et al. Research on the relationship between anti-skid performance and various aggregate micro texture based on laser scanning confocal microscope [J]. *Construction and Building Materials*, 2022, **316**: 125984. DOI: 10.1016/j.conbuildmat.2021.125984.
- [8] Zong Y, Li S, Zhang J, et al. Effect of aggregate type and polishing level on the long-term skid resistance of thin friction course [J]. *Construction and Building Materials*, 2021, **282**: 122730. DOI: 10.1016/j.conbuildmat.2021.122730.
- [9] Do M T, Tang Z, Kane M, et al. Evolution of road-surface skid-resistance and texture due to polishing [J]. *Wear*, 2009, **266** (5): 574 – 577. DOI: 10.1016/j.wear.2008.04.060.
- [10] Du Y, Qin B, Weng Z, et al. Promoting the pavement skid resistance estimation by extracting tire-contacted texture based on 3D surface data [J]. *Construction and Building Materials*, 2021, **307**: 124729. DOI: 10.1016/j.conbuildmat.2021.124729.
- [11] Takino H, Nakayama R, Yamada Y, et al. Viscoelastic properties of elastomers and tire wet skid resistance [J]. *Rubber chemistry and technology*, 1997, **70** (4): 584 – 594. DOI: 10.5254/1.3538445.
- [12] Copetti Callai S, Sangiorgi C. A review on acoustic and skid resistance solutions for road pavements [J]. *Infrastructures*, 2021, **6** (3): 41. DOI: 10.3390/infrastructures6030041.
- [13] Yun D, Tang C, Ran M, et al. Enveloping profile calculation method for enhancing the efficiency of pavement skid resistance prediction [J]. *Journal of Southeast University (Natural Science Edition)*, 2023, **53** (1): 130 – 136. DOI: 10.3969/j.issn.1001-0505.2023.01.016. (in Chinese)
- [14] Nayak S R, Mishra J, Palai G. Analysing roughness of surface through fractal dimension: A review [J]. *Image and Vision Computing*, 2019, **89**: 21 – 34. DOI: 10.1016/j.imavis.2019.06.015.
- [15] Issa M A, Issa M A, Islam M S, et al. Fractal dimension: A measure of fracture roughness and toughness of concrete [J]. *Engineering Fracture Mechanics*, 2003, **70** (1): 125 – 137. DOI: 10.1016/S0013-7944 (02) 00019-X.
- [16] Kokkalis A, Tsohos G, Panagouli O. Consideration of fractals potential in pavement skid resistance evaluation [J]. *Journal of Transportation Engineering*, 2002, **128** (6): 591 – 595. DOI: 10.1061/(ASCE)0733-947X (2002)128:6(591).
- [17] Peng Y, Li Q, Zhan Y, et al. Pavement skid resistance evaluation based on 3D areal texture characterization [J]. *Journal of Southeast University (Natural Science Edition)*, 2020, **50** (4): 667 – 676. DOI: 10.3969/j.issn.1001-0505.2020.04.010. (in Chinese)
- [18] Liu C, Zhan Y, Deng Q, et al. An improved differential box counting method to measure fractal dimensions for pavement surface skid resistance evaluation [J]. *Measurement*, 2021, **178**: 109376. DOI: 10.1016/j.measurement.2021.109376.
- [19] Chen Y, Wang K J, Zhou W F. Evaluation of surface textures and skid resistance of pervious concrete pavement [J]. *Journal of Central South University*, 2013, **20** (2): 520 – 527. DOI: 10.1007/s11771-013-1514-y.
- [20] Wang D, Chen X, Yin C, et al. Influence of different polishing conditions on the skid resistance development of asphalt surface [J]. *Wear*, 2013, **308** (1/2): 71 – 78. DOI: 10.1016/j.wear.2013.09.013.
- [21] Li P, Yi K, Yu H, et al. Effect of aggregate properties on long-term skid resistance of asphalt mixture [J]. *Journal of Materials in Civil Engineering*, 2021, **33** (1): 04020413. DOI: 10.1061/(asce)mt.1943-5533.0003539.
- [22] Qian Z, Hou Y, Dong Y, et al. An evaluation method for the polishing and abrasion resistance of aggregate [J]. *Road Materials and Pavement Design*, 2018, **21** (5): 1374 – 1385. DOI: 10.1080/14680629.2018.1546219.
- [23] Wang H, Wang C, Bu Y, et al. Correlate aggregate angularity characteristics to the skid resistance of asphalt pavement based on image analysis technology [J]. *Construction and Building Materials*, 2020, **242**: 118150. DOI: 10.1016/j.conbuildmat.2020.118150.
- [24] Woodward D, Millar P, Lantieri C, et al. The wear of stone mastic asphalt due to slow speed high stress simulated laboratory trafficking [J]. *Construction and Building Materials*, 2016, **110**: 270 – 277. DOI: 10.1016/j.conbuildmat.2016.02.031.
- [25] Yu H, Shen S, Qian G, et al. Packing theory and volumetrics-based aggregate gradation design method [J]. *Journal of Materials in Civil Engineering*, 2020, **32** (6): 04020110. DOI: 10.1061/(asce)mt.1943-5533.0003192.
- [26] Wang J, Kong Y, Fu T. Expressway crash risk prediction using back propagation neural network: A brief investigation on safety resilience [J]. *Accid Anal Prev*, 2019, **124**: 180 – 192. DOI: 10.1016/j.aap.2019.01.007.
- [27] Sollazzo G, Fwa T F, Bosurgi G. An ANN model to correlate roughness and structural performance in asphalt pavements [J]. *Construction and Building Materials*, 2017, **134**: 684 – 693. DOI: 10.1016/j.conbuildmat.2016.12.186.
- [28] Marcelino P, de Lurdes Antunes M, Fortunato E, et al. Machine learning approach for pavement performance prediction [J]. *International Journal of Pavement Engineering*, 2019, **22** (3): 341 – 354. DOI: 10.1080/10298436.2019.1609673.
- [29] Wang J, Luo T, Fu T. Crash prediction based on traffic platoon characteristics using floating car trajectory data and the machine learning approach [J]. *Accid Anal Prev*, 2019, **133**: 105320. DOI: 10.1016/j.aap.2019.105320.
- [30] Ye Z Y, Kim M K. Predicting electricity consumption in a building using an optimized back-propagation and Levenberg-Marquardt back-propagation neural network: Case study of a shopping mall in China [J]. *Sustainable Cities and Society*, 2018, **42**: 176 – 183. DOI: 10.1016/j.scs.2018.05.050.

[31] Chen C, Zhang G, Qian Z, et al. Investigating driver injury severity patterns in rollover crashes using support vector machine models [J]. *Accid Anal Prev*, 2016, **90**: 128 – 139. DOI: 10.1016/j.aap.2016.02.011.

[32] Scott W T, Stephen W W. Fractal scaling of soil particle-size distributions: Analysis and limitations [J]. *Soil Science Society of America Journal*, 1992, **56**: 362 – 369. DOI: 10.2136/sssaj1992.03615995005600020005x.

[33] Zhang T, Zhang C, Luo T. Effect of stress anisotropy on deformation and particle breakage of silica sand at high-pressure compression tests [J]. *Construction and Building Materials*, 2022, **316**: 125835. DOI: 10.1016/j.conbuildmat.2021.125835.

[34] Mokhtarimousavi S, Anderson J C, Azizinamini A, et al. Factors affecting injury severity in vehicle-pedestrian crashes: A day-of-week analysis using random parameter ordered response models and Artificial Neural Networks [J]. *International Journal of Transportation Science and Technology*, 2020, **9**(2): 100 – 115. DOI: 10.1016/j.ijtst.2020.01.001.

[35] Zhang Z, He H, Yu C, et al. Using the modified two-mode method to identify surface water in Gaofen-1 images [J]. *Journal of Applied Remote Sensing*, 2019, **13**(2): 022003. DOI: 10.1117/1.JRS.13.022003.

[36] Feng J, Zhang H, Gao K, et al. Efficient creep prediction of recycled aggregate concrete via machine learning algorithms [J]. *Construction and Building Materials*, 2022, **360**: 129497. DOI: 10.1016/j.conbuildmat.2022.129497.

[37] Roy N, Sarkar S, Kuna K K, et al. Effect of coarse aggregate mineralogy on micro-texture deterioration and polished stone value [J]. *Construction and Building Materials*, 2021, **296**: 123716. DOI: 10.1016/j.conbuildmat.2021.123716.

[38] Peng Y, Li J Q, Zhan Y, et al. Finite element method-based skid resistance simulation using in-situ 3D pavement surface texture and friction data [J]. *Materials (Basel)*, 2019, **12** ( 23 ): 3821. DOI: 10.3390/ma12233821.

基于集料力学特征与级配分形的沥青混合料抗滑衰变预测

孔令云<sup>1,2</sup> 曾启岚<sup>1,2</sup> 张政奇<sup>1,2</sup> 彭 毅<sup>3</sup> 王大为<sup>4</sup> 余 苗<sup>1,2</sup> 战 友<sup>5</sup>

(<sup>1</sup>重庆交通大学交通土建工程材料国家地方联合工程实验室,重庆 400074)  
(<sup>2</sup>重庆交通大学土木工程学院,重庆 400074)  
(<sup>3</sup>重庆交通大学交通运输学院,重庆 400074)  
(<sup>4</sup>哈尔滨工业大学交通科学与工程学院,哈尔滨 150090)  
(<sup>5</sup>西南交通大学土木工程学院,成都 610031)

**摘要:**以粗集料的力学指标、分形维数以及 BPN 作为研究对象进行数据采集,基于前馈神经网络算法与支持向量机算法,提出了一种新型路面抗滑性能预测模型.采用加速加载试验,记录沥青混合料在轮载作用下表面抗滑性能的衰减过程,并利用指数模型对轮载次数与 BPN 的数值关系进行拟合.通过灰色关联度分析和相关性分析,评估各项因素对沥青路面抗滑性的影响程度.基于主成分分析结果,设计了 6 种方案,用于前馈神经网络算法和支持向量机算法的训练、验证和测试.结果表明,不同类型集料呈现出不同的抗滑性能,石英砂岩最佳,玄武岩次之,石灰岩较差.磨光值与沥青抗滑性能衰减模型的关联性最高.前馈神经网络算法构建的模型表现更为稳定, $R^2$  值约为 0.8,展现出良好的预测能力.

**关键词:**加速加载;抗滑性能;指数模型;前馈神经网络;支持向量机

**中图分类号:**U416.217